

Synthesis and Characterization of Hydroxyapatite/Titania Composite and Its Application on Photocatalytic Degradation of Remazol Red B Textile Dye Under UV Irradiation

I Nyoman Sukarta^{1*}, I Dewa Ketut Sastrawidana¹

¹ Chemistry Department, Faculty of Mathematics and Natural Sciences, Universitas Pendidikan Ganesha, Singaraja 81117 Bali, Indonesia

* Corresponding author's e-mail: nyoman.sukarta@undiksha.ac.id

ABSTRACT

This research was conducted to synthesize and characterize hydroxyapatite-titania (HA/TiO₂) composites and test their photocatalytic degradation activity on the remazol red RB textile dye. The chemical precipitation method was utilized to produce hydroxyapatite (HA) based on the conversion of calcium carbonate presented in sea mussel shells into calcium oxide with a calcination temperature of 1000°C for 2 hours and then followed by the addition of phosphorous acid at pH medium of 11 and sintered at 700°C to obtain an HA crystal. The HA/TiO₂ composite at variation weight of HA and TiO₂ ratio were prepared with hydrothermal technique and characterized by the FTIR spectroscopy, X-ray diffraction, and scanning electron with energy dispersive X-ray spectroscopy. A total of 250 mL of 50 mg/L Remazol red RB dye solution was photocatalytically removed using a HA/TiO₂ composite irradiated with 25 Watt UV light and using the adsorption method. Characterization results using FTIR, XRD, and SEM-EDX show that the synthesized hydroxyapatite (HA) has a degree of crystallinity of 68% with a Ca/P ratio of 1.66. The highest degradation efficiency of 250 mL of remazol red RB with a concentration of 50 mg/L was achieved at 94.22% in 2 hours of contact time by a photocatalysis treatment employing the HA/TiO₂ composite at a ratio of 1:1 in comparison to only 92.23% removal by the HA adsorption process.

Keywords: hydroxyapatite/TiO₂ composite, remazol red RB, sea mussel shells, photocatalytic degradation.

INTRODUCTION

The existence of wastewater generated from the textile industry is an environmental problem that needs great attention. The wastewater from various textile industries has a high content of organic matter, pH value, dyes, detergents, Heavy metals, chemical oxygen demand (COD), and biochemical oxygen demand (BOD), and chemical auxiliaries that could potentially have a negative impact on humans and the environment (Azanaw et al., 2022; Akuma et al., 2022). According to estimates, the use of azo dyes is reaching 60–70% of all of the dyes utilized in the textile sector. An example of azo dye is remazol red RB, which is commonly used in dyeing cotton, wool, and silk fabrics. Most of the azo dyes are toxic, mutagenic and carcinogenic

to living things, including humans (Siddiqui et al., 2023). Commonly, the textile effluent contains dyes with different concentrations from 10–250 mg/L (Ghaly et al., 2014). Therefore, it must be treated to meet wastewater quality standards before being discharged into the environment.

A various techniques have been developed for removing pollutants and dyes from textile wastewater which include electrochemical oxidation (Latha et al., 2017; Sastrawidana et al., 2018; Ojha and Shrivastav., 2023), adsorption (Alarcón et al., 2022; Musthofa et al., 2023), coagulation (Raj et al., 2023), membrane (Al-Sultan et al., 2022; Reddy et al., 2022), ozone (Al-Rubaiey et al., 2022), photocatalytic (Sahoo et al., 2022), and biodegradation using fungi (Sukarta et al., 2021; Sudiana et al., 2022).

Among the available technologies, photocatalytic degradation is a promising method for the remediation of textile wastewater due to its high degradation efficiency, low toxicity, low maintenance, and environmentally friendly technology (Ren et al., 2021; Mancuso and Lervolino, 2022). Basically, photoexcitation of semiconductors by a photon energy with electrons are excited from the valence band to the conduction band when there is enough energy. The reactive species produced by photoexcitation, such as peroxide (H_2O_2), superoxide ion ($\bullet O_2^-$), and hydroxyl radical ($OH\bullet$), are crucial to the breakdown of pollutants in water (Vital-Grappin et al., 2021). Photocatalysis uses a suitable catalyst that is irradiated with unlimited ultraviolet and visible light radiation, can destroy pollutants through oxidation-reduction reactions (Rajabi et al., 2020). Photocatalytic reactions can mineralize the organic pollutant materials into CO_2 and water without requiring expensive oxidizing chemicals (Sirajudheen et al., 2021). Some of the catalysts used for photocatalytic degradation of dyes include Ce-TiO₂ catalysts (Touti et al., 2016), catalyst composites of polyaniline (Oyetade et al., 2022), and green zinc oxide nanoparticles synthesized in plant extract (Dihom et al., 2022).

Titanium dioxide (TiO₂) has been widely used as a photocatalytic material because of its specific properties, such as having high photocatalytic activity, non-toxicity, chemical stability, ease of obtaining in the market and its ability to decompose various organic compounds (Hayashi et al., 2020; Mirkovic et al., 2022). However, in practical applications, the TiO₂ powder is difficult to recover because it is suspended in wastewater. Thus, immobilizing TiO₂ on suitable support materials is important and required. Some support materials that have been studied to immobilize TiO₂ include silica granules, natural zeolite, activated carbon, and hydroxyapatite (Barakat et al., 2023; Wardhani et al., 2016; Odabasi et al., 2022; Syafira et al., 2023). Recently, the use of greener materials, such as hydroxyapatite (HA) has been studied in catalyst-support applications due to its outstanding chemical stability, bioactivity, and biocompatibility (Chong et al., 2018). Besides that, HA with the chemical formula $Ca_{10}(PO_4)_6(OH)_2$ has a large specific surface area and thermal stability, making it a good supporting catalyst material (Nguyen et al., 2022).

Apart from being used as an adsorbent and supporting catalyst in wastewater bioremediation, HA is widely used for biomedical applications

such as for drug delivery systems, medical devices, and implant material with application in dentistry (Izzetti et al., 2022). Considering the wide application of hydroxyapatite, production and searching for raw materials from natural sources should be done continuously. The natural materials that can be used for HA synthesis are those that are rich in calcium, either from biological sources such as mammal bones, fish bones, egg shells, coral, and shellfish or from inorganic materials, such as limestone (Wu et al., 2023; Kumar et al., 2020; Arif et al., 2020).

Blood sea mussel (*Anadara granosa*) is a genus of Anadara that is commonly found in the sea water of Bali. In general, the protein content of mussels ranged from 59.07 to 68.31% by weight (Naik et al., 2020). Because of their high nutrient content, the meat of sea shells is a favorite food, while their shells are discharged and become a waste in the environment. The content of calcium carbonate in blood mussel shells is estimated at 98% by weight (Asmawathi et al., 2018), which makes them potential as raw materials for hydroxyapatite synthesis. This is an innovative way to utilize waste into valuable products, which is also a course of action to reduce mussel shell waste in the environment.

The aim of this research was to synthesize HA from sea mussel shells through a chemical precipitation method. The HA synthesized is characterized and then used as a support material for the TiO₂ catalyst. The HA/TiO₂ composite was analyzed for its surface morphology and used for photocatalytic degradation of remazol red RB dye irradiated with 25-watt UV light.

MATERIALS AND METHODS

Materials

For the synthesis of HA and HA/TiO₂ composites, the following reagents were used: orthophosphoric acid (H_3PO_4), titanium dioxide (TiO₂), and ammonia (NH₃). All reagents are analytical-grade reagents purchased from Sigma-Aldrich. In turn, samples of sea mussel shells as a source of calcium carbonate (CaCO₃) were obtained from sea waters in Bali. Orthophosphoric acid and calcium oxide (CaO) were used as precursors, and ammonia was used for the pH adjustment of the medium. The chemical composition of Remazol red (RB) is shown in Figure 1.

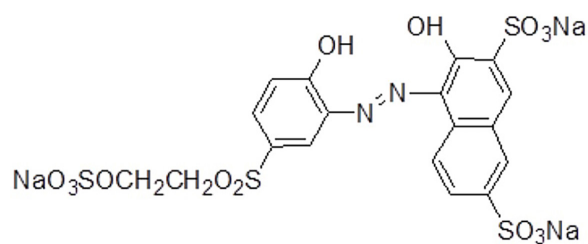


Figure 1. The remazol red RB dye chemical composition

Calcination of sea mussel shell

After removing any contaminants from the surface with distilled water, the sea mussel shells were crushed in a crusher. A furnace was used to calcine the shell powder for two hours at 1000 °C to convert the calcium carbonate (CaCO_3) into calcium oxide (CaO).

Preparation of hydroxyapatite

HA was prepared using the chemical precipitation method according to the procedure described by Cahyaningrum et al., 2017. In order to prepare HA, 100 g of CaO was droppedwise at a rate of 1 mL/min into 350 mL of deionized water along with 38.4 mL of a 96% H_3PO_4 solution. After adding 33% ammonia solution to bring the mixture pH to 11, it was heated to about 80 °C and continuously stirred with a magnetic stirrer for 24 hours at room temperature. To extract the HA precipitate, the mixture was agitated for a full day and then filtered through Whatman filter paper number 42. For six hours, the HA precipitate was dried at 80 degrees Celsius in an oven, then it was crushed to create HA powder. Ultimately, a furnace was used to sinter the generated HA for two hours at a temperature of 700 °C in order to produce HA dry crystal.

Preparation and characterization of the HA/TiO₂ composite

The composite of HA/TiO₂ was made by mixing HA powder and TiO₂ (anatase, 98.0–100%, CAS 13463-67-7, Merck KGaA, Made in Germany) with weight variation ratios of 1:1, 2:1, 3:1, 4:1 and 5:1, respectively. The mixtures were added with one hundred mL of de-ionized water while being swirled for 24 hours with a magnetic stirrer. The mixtures were allowed to rest for 48 h to obtain the precipitate of the HA/

TiO₂ composite. After that, the formed HA/TiO₂ composite powder was calcined at 700 °C for 2 h to obtain HA/TiO₂ dried crystal. The composites of HA and TiO₂ were described by identifying the functional groups with FTIR, measuring the degree of crystallinity using XRD, surface morphology, distribution of TiO₂ on the HA surface and the atomic ratio of Ca/P with SEM-EDX spectroscopy.

Remazol red RB photocatalytic degradation in natch

The setup for the textile dye Remazol Red RB batch photocatalytic degradation process was shown in Figure 2.

The photocatalytic reactor with dimension of length x width x height is 35×13×13 cm, respectively. UV light 25 Watt was used as a source of photon energy in degradation process of remazol red RB textile dye. To maintain the homogeneity of the electrolyte distribution, 500 mL of dye solution at a concentration of 50 mg/L was added to the photocatalytic degradation reactor and continuously stirred at 150 rpm using an automatic magnetic stirrer. At an interval of 15 minutes for 2 hours, A sample of 15 milliliters was obtained, and after the suspended particles were separated, its absorbance was measured at the wavelength of 516.5 nm. Degradation efficiency of remazol red RB by photocatalytic and adsorption processes at different weight ratio of HA/TiO₂ were investigated. The degradation efficiency is calculated using the following equation:

$$\begin{aligned} \text{Degradation efficiency}(\%) &= \\ &= \frac{A_o - A_i}{A_o} \times 100\% \end{aligned} \quad (1)$$

where: A_o is the initial absorbance of dye;
 A_i is absorbance of dye after treatment at certain times.

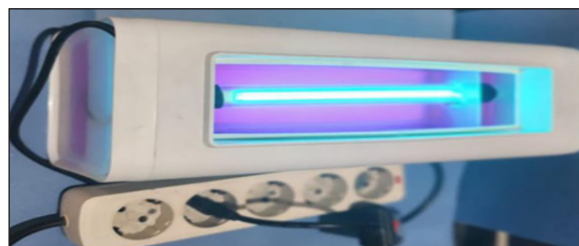
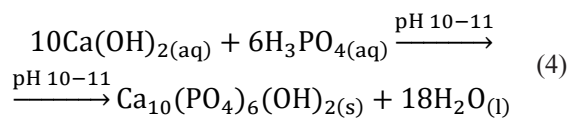
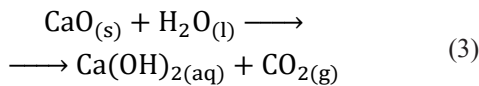
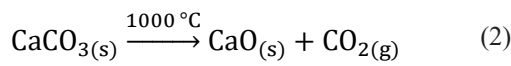


Figure 2. Performance of photocatalytic degradation reactor set up

RESULTS AND DISCUSSIONS

Sea mussel shells contains calcium carbonate accounts for 95–98% by weight (Borciani et al., 2023). This amount of calcium carbonate has the potential as raw materials resources for hydroxyapatite synthesis. Calcination of sea mussel shell to convert CaCO_3 into CaO was done through the following reaction:



FTIR analysis

The FTIR spectra of HA, TiO_2 , and HA/ TiO_2 were captured in the 4000–500 cm^{-1} wavelength region on an IR Affinity-1 from Shimadzu. The Fourier transform infrared spectra of HA/ TiO_2 composite samples generated at varying HA to TiO_2 weight ratios are shown in Figure 3.

Figure 3 shows the FTIR spectra of HA, TiO_2 and composites of HA/ TiO_2 with distinct weight ratio of HA to TiO_2 and the characteristic of

absorption band are shown in Table 1. The typical characteristic bands at 3572.17 cm^{-1} and 3647.39 cm^{-1} for all samples indicate stretching vibrations of hydroxyl groups (OH). The bands are located at around 1049 cm^{-1} and 1091 cm^{-1} corresponding to asymmetric stretching mode of vibration of P-O bond from PO_4^{3-} anion of apatite (Solonenko et al., 2022), and the appearance peaks at 632.65 cm^{-1} , 603.72 cm^{-1} and 561.29 cm^{-1} for all the samples also indicates to symmetric P-O stretching vibration of PO_4^{3-} group (Kumar et al., 2021). Al-Hamdan et al., 2020, also states that the powerful 560 cm^{-1} peaks and around 1017 cm^{-1} indicate hydrogen phosphate (HPO_4) and phosphate (PO_4), in that order. The absorption band at 1456.26 cm^{-1} was assigned to ion of carbonate (CO_3^{2-}) in accordance with the results of Dermawan et al., 2022 who stated that groups of carbonate ions were observed in the range of 1500–1400 cm^{-1} wave-numbers. In addition, the frequency bands around 2358 cm^{-1} and 2353 cm^{-1} can be ascribed to CO_2 vibration (Ummartyotin and Tangnorawich., 2015). From the FTIR analysis, the precipitated powders were proven to be hydroxyapatite. The peak of absorption observed at 690.51 cm^{-1} shows the Ti-O stretch band, which is a typical TiO_2 peak. According to Alobaidi and Alwared, 2022, the fundamental absorption bands of Ti-O-T and Ti-O vibrations are found within the 400–700 cm^{-1} range.

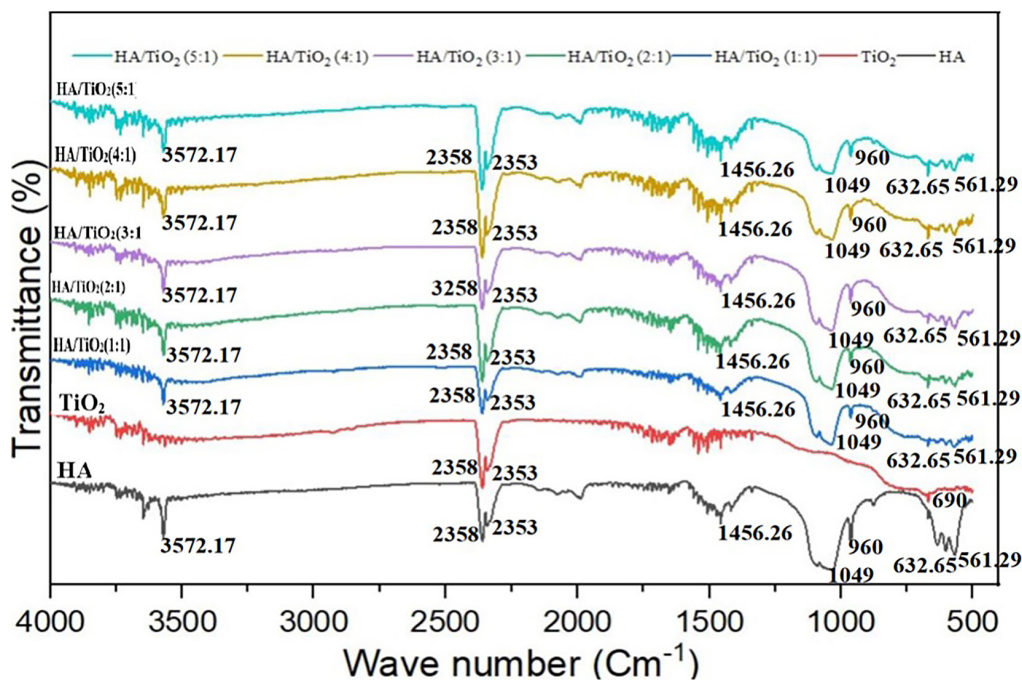


Figure 3. FTIR spectra of HA, TiO_2 and composites of HA/ TiO_2

Table 1. Types of vibration of HA, TiO₂, and HA/TiO₂ composite

Wavenumber (cm-1)	Vibration mode	Functional group
3572.17	OH Stretching	Hydroxyl group
3647.39	OH Stretching	Hydroxyl group
2358	CO ₂ bending	CO ₃ ²⁻ group
2353	CO ₂ bending	CO ₃ ²⁻ group
1456.26	Asymmetric stretching	CO ₃ ²⁻ group
1091	PO ₄ bending	Phosphate group
1049	PO ₄ bending	Phosphate group
960	PO ₄ bending	Phosphate group
690.51	Ti-O stretching	TiO ₂ group
632.65	PO ₄ bending	Phosphate group
603.72	P-O stretching	Phosphate group
561.29	P-O stretching	Phosphate group

X-ray diffraction analysis

The crystallinity degree of the prepared composites of HA/TiO₂ at different weight ratio of HA to TiO₂ such as 1:1; 2:1; 3:1; 4:1 and 5:1 was identified using X-ray diffraction (XRD) spectroscopy. The prepared HA, TiO₂ XRD patterns and composites of HA/TiO₂ are shown in Figure 4, while the results of the calculated crystallite size and crystallinity degree using origin 8.5 Pro. software are listed in Table 2.

Figure 4 shows the patterns of XRD of the HA powder, pure powder of TiO₂, and HA/TiO₂ different composition. The XRD spectrum patterns of HA was obtained at position 2θ were 25.591, 31.874, 32.283, 39.917, 46.801 and 49.557, respectively. These peaks match the characteristic

peaks of HA based on JCPDS No. 09.0432, in which appears at 2θ = 25.8 (002), 31.7 (211), 32.9 (300), 46.7 (222) and 49.4° (213). According to Ahmed et al., 2015, the hexagonal structure of HA is characterized by the appearance of a strong diffraction peak at position 2θ around of 31.780 together with two other peaks around of 32.266°. In addition, the diffraction peaks at 2θ around of 25.9°, 31.8°, 46.7° and 49.5° are typical for pure HA, while for TiO₂, the peaks observed at 2θ around of 25.3°, 37.8° and 48.0° are representative for anatase TiO₂ (Noviyanti et al., 2022; Fatimah et al., 2023). The results of XRD analysis of TiO₂ are in good agreement with Jamil et al., 2022 who stated that the 2θ at peak 25.491° and 54.30° which confirms the TiO₂ anatase structure.

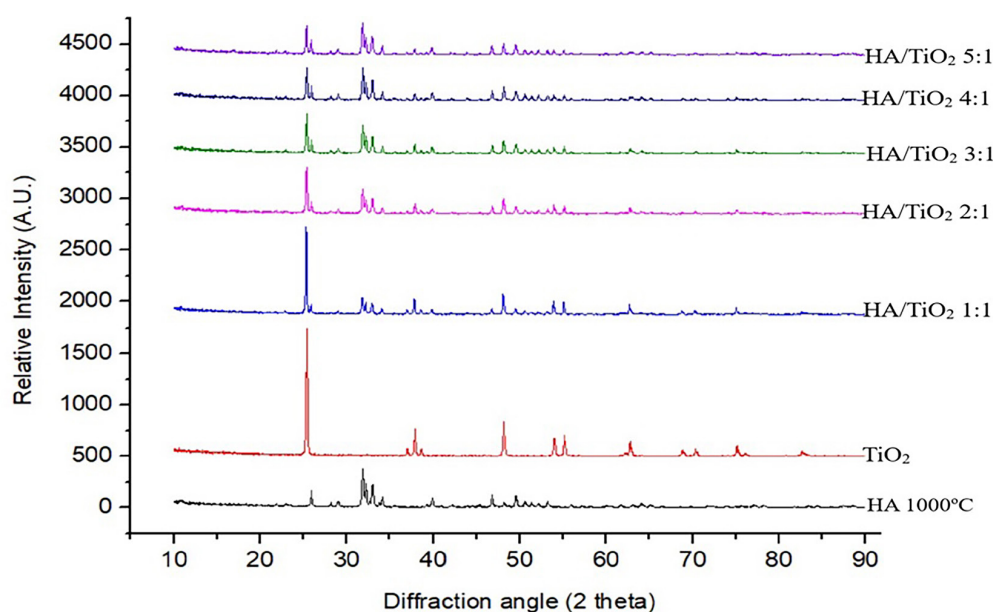
**Figure 4.** The patterns of XRD of HA, TiO₂ and composites of HA/TiO₂

Table 2. Crystallinity of the HA, TiO₂ and HA/TiO₂ composites

Sample	Peak position (°2Th)	FWHM (°2 Th)	Crystallinity (%)
HA	31.874	0.1574	68
TiO ₂	25.398	0.1378	73
HA/TiO ₂ (1:1)	25.323	0.1581	63
HA/TiO ₂ (2:1)	25.373	0.1771	56
HA/TiO ₂ (3:1)	25.386	0.1968	60
HA/TiO ₂ (4:1)	31.858	0.0787	57
HA/TiO ₂ (5:1)	31.841	0.1968	57

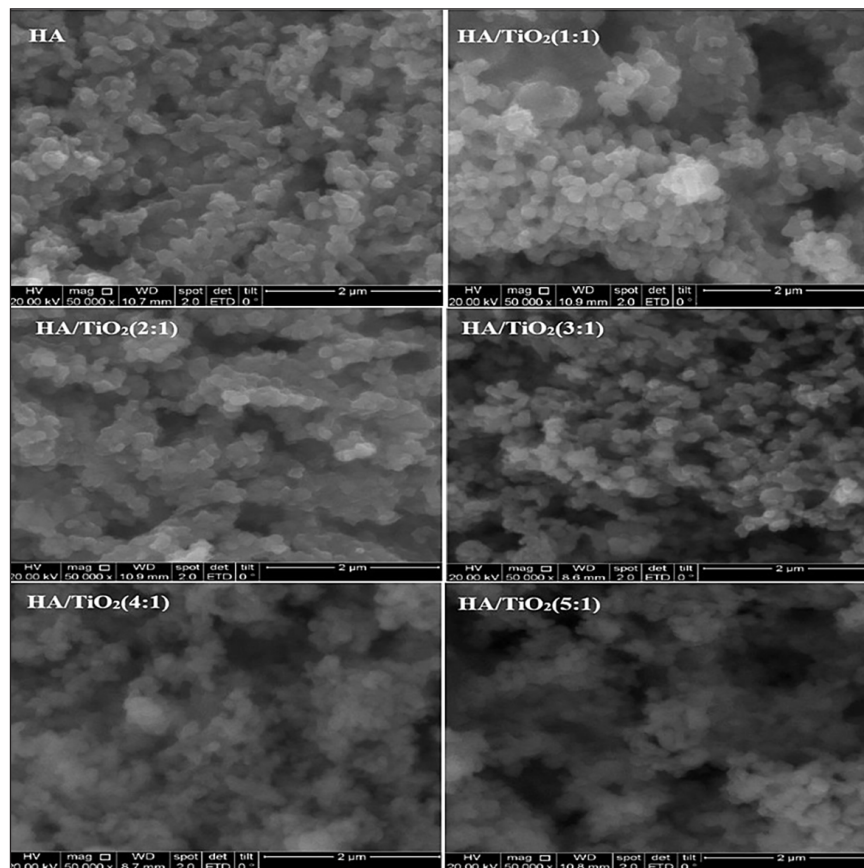
XRD pattern of the HA/TiO₂ shows peaks corresponding to HA and TiO₂ anatase. The diffraction peak at $2\theta=25.59, 31.87, 46.80$ and 49.56 are typical peaks from HA, while the peaks of TiO₂ were noticeable at $2\theta=25.39, 37.8$ and 48.0 . The peak intensity of TiO₂ increased along with the TiO₂ content as well as the peak of HA increased with increasing HA content in HA/TiO₂ composites.

The crystallinity of HA, TiO₂, and composites of HA/TiO₂ was analyzed based on the peaks in the XRD pattern, and then using Origin 8.5 Pro software, the crystallinity percentage of each composite sample can be calculated. From the Table 2, it is known that HA/TiO₂ 1:1 composites have the highest percentage crystallinity compared to other

composites of HA/TiO₂. However, the composites of HA/TiO₂ prepared had lower crystallinity than pure HA and TiO₂. The material with a high degree of crystallinity will be more stable and have strong mechanical properties, making it suitable for application as a catalyst support or as an adsorbent.

Analysis of SEM-EDX

The morphology and element content of the HA samples were assessed using SEM-EDX, both before and after they were impregnated with various masses of TiO₂. The representative scanning electron micrographs of the TiO₂, HA and HA/TiO₂ at different TiO₂ contents after sintering

**Figure 5.** SEM images of HA and HA/TiO₂ composites with different mass ratio of HA to TiO₂

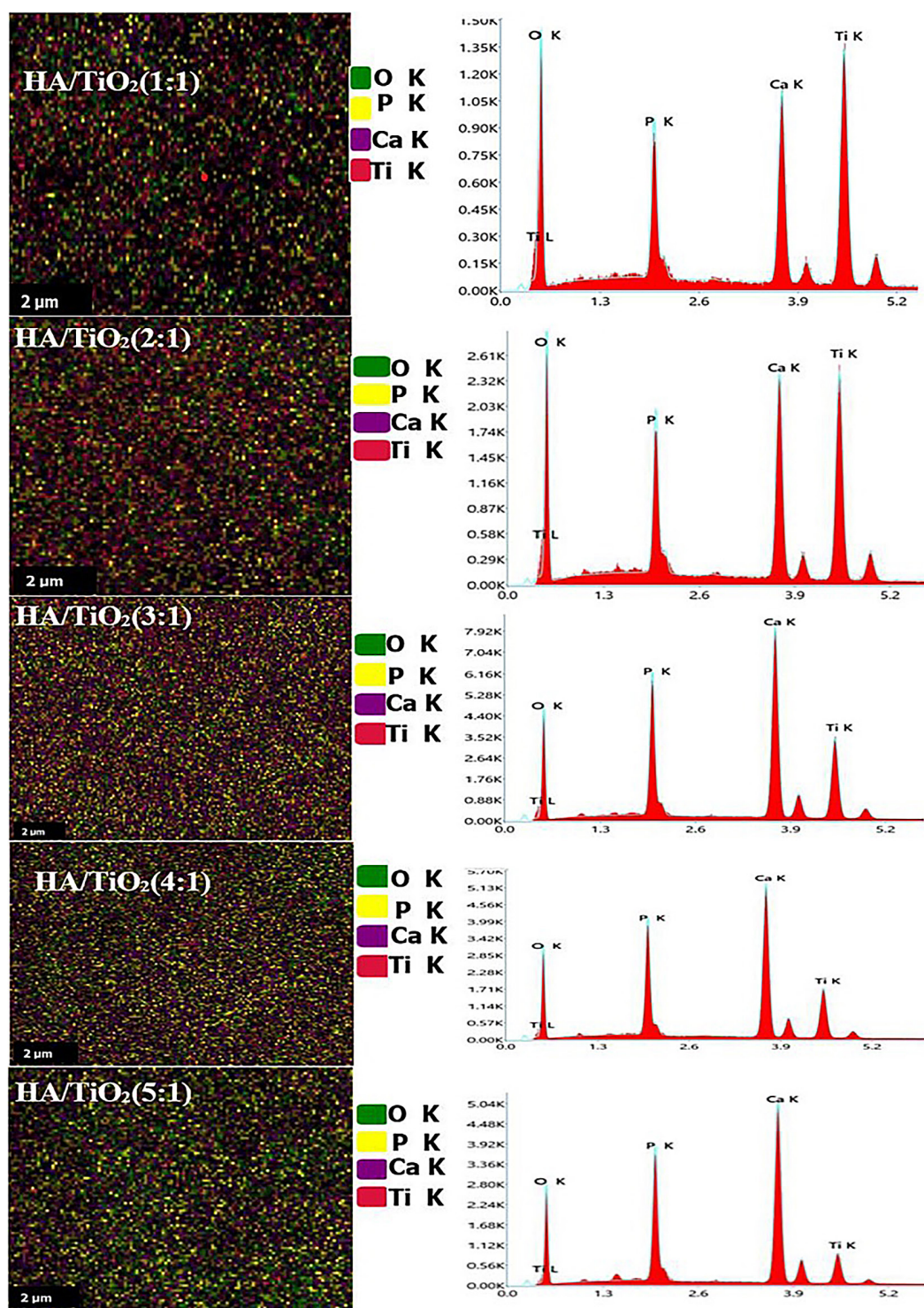


Figure 6. EDX of HA and composite of HA/TiO₂ with different ratio of HA to TiO₂

Table 3. Calcium/phosphate atomic ratio of HA and HA/TiO₂ composites

Component	HA At, %	HA/TiO ₂ 1:1 (At, %)	HA/TiO ₂ 2:1 (At, %)	HA/TiO ₂ 3:1 (At, %)	HA/TiO ₂ 4:1 (At, %)	HA/TiO ₂ 5:1 (At, %)
Ti	-	11.0	10.0	7.1	5.6	3.3
O	75.8	76.7	76.7	71.1	71.8	71.0
Ca	15.1	7.6	8.4	14.2	14.7	17.1
P	9.10	4.6	4.9	7.6	7.9	8.6
Ca/P	1.66	1.65	1.71	1.87	1.86	1.99

at 700 °C are shown in Figure 5 and the Ca/P ratio is presented in Table 3.

Figure 5 shows the surface morphology of pure HA from sea mussel shells and HA/TiO₂ composite. From the SEM images it can be seen that TiO₂ impregnated on the HA surface covers the pores of the hydroxyapatite.

On the basis of the data displayed in Figure 6, the EDX analysis of the HA/TiO₂ composite comprises oxygen, calcium, phosphorus and titanium where the uniform distribution of TiO₂ particles over the HA surface. In addition, the presence of Ti and O peaks in EDX spectrum reflects that TiO₂ particles are incorporated into the HA matrix.

Table 3 represents the composition of elements in synthesized HA/TiO₂ composites with their corresponding Ca/P ratio obtained by energy dispersive X-ray analysis. The Ca/P atomic ratio for sample HA, HA/TiO₂ 1:1, HA/TiO₂ 2:1, HA/TiO₂ 3:1, HA/TiO₂ 4:1, and HA/TiO₂ 5:1 was calculated from EDX, and its results were found to be 1.66, 1.65, 1.71, 1.87, 1.86, and 1.99, respectively. The atomic ratio of Ca/P in HA was 1.66, which was closest to the stoichiometric Ca/P ratio of 1.667 in HA. However, the Ca/P atomic ratio changes when composited with TiO₂.

Degradation studies

The degradation test of the HA and HA/TiO₂ composites was examined against remazol red RB textile dye solutions. The degradation process was conducted by two treatments, namely photocatalysis and adsorption. The degradation

efficiency of remazol red RB through the adsorption process is shown in Figure 7, whereas photocatalysis is presented in Figure 8.

As it can be seen in Figure 7, the degradation of remazol red RB through the adsorption process was more effective when using HA compared to the composite of HA/TiO₂. In adsorption, the degradation rate of the remazol red RB increases from 15 to 60 minutes, and then the adsorption efficiency increases insignificantly until the process continues up to 120 minutes of contact time. The degradation efficiency of red RB using HA was 91.25% within 60 minutes and then achieved 92.23% after 120 minutes of contact time. This result is consistent with earlier studies conducted by Pai et al., 2022, in which they found an adsorption efficiency of 94.38% by hydroxyapatite/magnetite nanocomposites at a 54 mg/L starting concentration of acid blue. Adsorption studies done by Aaddouz et al., 2023 also found that a removal efficiency of 88.88% was achieved at a 45 mg/L starting methylene blue concentration and a 20-minute contact period.

Figure 8 displays the photocatalysis activity of the HA/TiO₂ composite against remazol red RB textile dye. It is clearly observed that 94.22% of remazol red RB was photocatalysis degraded using HA/TiO₂ 1:1 composite after 120 minutes of contact time under UV irradiation of 25 W. The photocatalytic activity rate decreased with the lower content of TiO₂ impregnated in HA. The degradation efficiency of 250 mL of remazol red RB dye with 50 mg/L concentration using HA, TiO₂, HA/TiO₂ 1:1, HA/TiO₂ 2:1, HA/TiO₂ 3:1, HA/

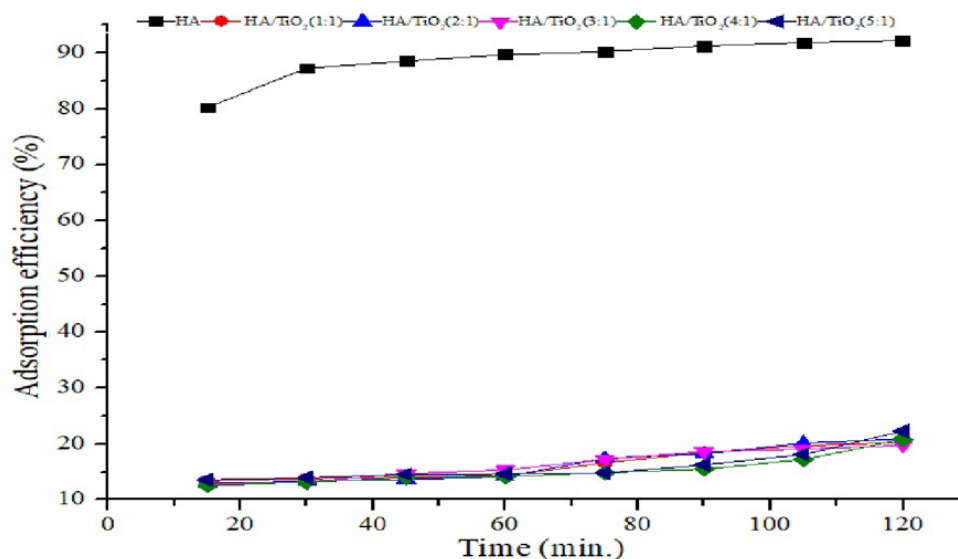


Figure 7. Adsorption of remazol red RB by HA and composites of HA/TiO₂

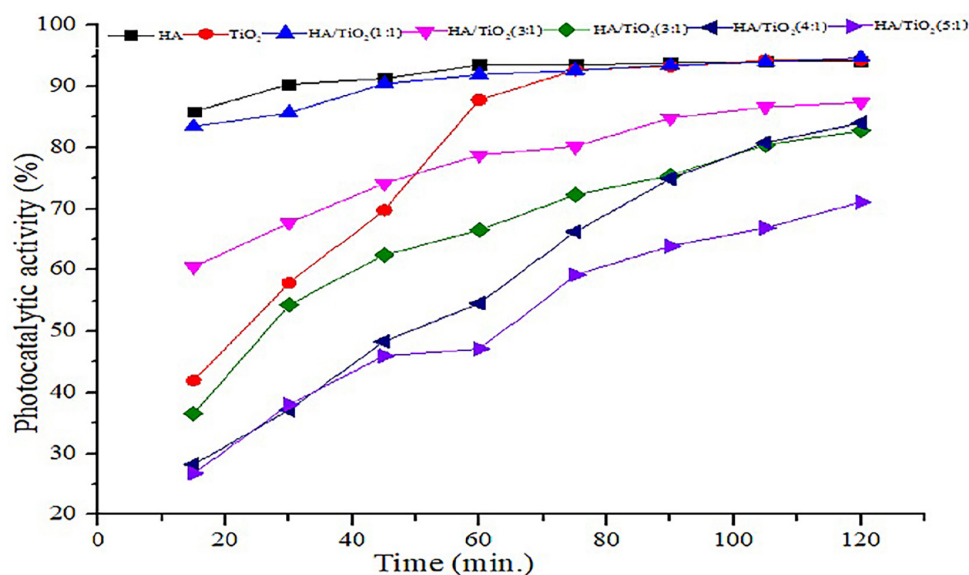


Figure 8. Photocatalysis degradation activity of HA/TiO₂ composites against remazol red RB

TiO₂ 4:1, and HA/TiO₂ 5:1 under UV light of 25 W irradiation for 120 minutes of contact time was obtained at 94.13%, 94.39%, 94.22%, 87.38%, 82.73%, 84.05% and 71.08%, respectively. On the other hand, the degradation efficiency using HA, HA/TiO₂ 1:1, HA/TiO₂ 2:1, HA/TiO₂ 3:1, HA/TiO₂ 4:1, and HA/TiO₂ 5:1 through adsorption was 92.23%, 20.25%, 20.87%, 19.7%, 20.86%, and 22.28%. This finding is higher than Qutub et al., 2022, who found that the photocatalytic degradation efficiency of the CdS/TiO₂ nanocomposite against acid blue 29 dye with a concentration of 0.06 mM was 84% under visible light irradiation for 90 min. Another study conducted by Hossain et al., 2022 also found that a photocatalytic degradation efficiency of 99% was obtained when removing 50 mL of Congo red dye at 20 mg/L concentration using a Cu/TiO₂ nanocomposite with an irradiation time of 180 minutes.

CONCLUSIONS

In this study, the synthesis and characterization of hydroxyapatite from sea mussel shells and its use as a supporting catalyst of TiO₂ for remazol red RB of photocatalytic degradation under irradiation of UV light was investigated. The crystalline features of HA and HA/TiO₂ were investigated through XRD analysis that indicated the formation of hexagonal structure of HA/TiO₂. It was confirmed via SEM-EDX analysis, The uniform distribution of TiO₂ over hydroxyapatite and the Ca/P ratio in hydroxyapatite and hydroxyapatite/ titanium oxide

composite were obtained in the range of 1.66-1.99 approach to the Ca/P ratio the theoretical value characteristic of stoichiometric hydroxyapatite. The degradation efficiency of the 1:1 HA/TiO₂ composite against 500 mL of Remazol Red RB with a concentration of 50 mg/L through a photocatalytic reaction irradiated with 25 Watt UV light was achieved at 94.22% in 120 minutes, while the efficiency of 92.23% was achieved using HA through the adsorption process.. Thus, hydroxyapatite prepared from the sea mussel shell can be effectively utilized as excellent non-toxic and cheaper natural supporting catalyst and also used as bioadsorbent for the removal of dye from aqueous medium.

Acknowledgments

This research was financially supported by the Directorate Research and Community Service, The Minister of Education, Culture, Research and Technology of Indonesia with contract number of 1512/UN48.16/LT/2023. All the authors thank the research and community service of Universitas Pendidikan Ganesha for providing of administration facilities service.

REFERENCES

1. Aaddouz M., Azzaoui K., Akartasse, N., Mejdoubi E., Hammouti B., Taleb M., Sabbahi R., Alshaha-teet S.F. 2023. Removal of methylene blue from aqueous solution by adsorption onto hydroxyapatite nanoparticles. *J. Mol. Struct.* 1288: 135807. <https://doi.org/10.1016/j.molstruc.2023.135807>

2. Ahmed Y.M.Z., El-Sheikh S.M., Zaki Z.I. 2015. Influence of heat treatment and dispersing agent addition on hydroxyapatite powder properties and its suspension characteristics. *Asian J. Chem.* 27(7): 2608–2618. <http://dx.doi.org/10.14233/ajchem.2015.18543>
3. Akuma D.A., Hundie K.B., Bullo T.A. 2022. Performance improvement of textile wastewater treatment plant design by STOAT model simulation. *Environ. Health Eng. Manag. J.* 9(3): 213–221. <https://doi.org/10.34172/EHEM.2022.22>
4. Alarcón M.A.D.F., Pacheco C.R., Bustos K.G., Meza K.T., Terán-Hilares F., Tanaka D.A.P., Andrade G.J.C., Terán-Hilares R. 2022. Efficient dye removal from real textile wastewater using orange seed powder as suitable bio-adsorbent and membrane technology. *Water.* 14:1–14. <https://doi.org/10.3390/w14244104>
5. Al-Hamdan R.S., Almutairi B., Kattan H.F., Alre-sayes S., Abduljabbar T., Vohra F. 2020. Assessment of hydroxyapatite nanospheres incorporated dentin adhesive. A SEM/EDX, micro-Raman, microtensile and micro-indentation study. *Coatings.* 10(12):1–12. <https://doi.org/10.3390/coatings10121181>
6. Alobaidi T.B., Alwared A.I. 2022. Biosynthetic of Titanium Dioxide Nanoparticles Using *Zizyphus Spina-Christi* Leaves Extract: Properties. *J. Ecol. Eng.* 23(1): 315–324. <https://doi.org/10.12911/22998993/143971>
7. Al-Rubaiey N.A. 2022. A trend in ozone treatment of wastewater: A Review. *Iraqi J. Oil Gas Res.* 2(1): 55–64. <http://doi.org/10.55699/ijogr.2022.0201.1016>
8. Al-Sultan A.A., Kadhim R.J., Al-Emami O.H., Al-salhy Q.F., Majdi H.S. 2022. Optimization of graphene oxide mixed matrix membrane for AB-210 dye removal. *J. Ecol. Eng.* 23(9): 115–127. <https://doi.org/10.12911/22998993/151746>
9. Arif S., Hermana G.N., Khalida Z., Arif M.W., Puspita I. Synthesis of biomaterial hydroxyapatite from limestone by using two-step conversion. *Int. J. Sci. Eng. Inf. Technol.* 5(1): 236–238.
10. Asmawati A., Thalib B., Thalib A.M., Reni D.S., Hasyim R. 2018. Comparison of blood clam (*Anadara granosa*) shell paste, shrimp (*Litopenaeus vannamei*) shell paste and casein phosphopeptide-amorphous calcium phosphate (CPP-ACP) paste as teeth remineralization material. *J. Dentomaxillofacial Sci.* 3(3): 162–165. <https://doi.org/10.15562/jdmfs.v3i3.834>
11. Azanaw A., Birlie B., Teshome B., Jemberie M. 2022. Textile effluent treatment methods and eco-friendly resolution of textile wastewater. *Case Stud. Chem. Environ. Eng.* 6:100230. <https://doi.org/10.1016/j.cscee.2022.100230>
12. Barakat N.A.M., Irfan O.M., Mohamed O.A. 2023. TiO₂ NPs-immobilized silica granules: New insight for nano catalyst fixation for hydrogen generation and sustained wastewater treatment. *PLoS One.* 18(6): e0287424. <https://doi.org/10.1371/journal.pone.0287424>
13. Borciani G., Fischetti T., Ciapetti G., Montessissa M., Baldini N., Graziani G. 2023. Marine biological waste as a source of hydroxyapatite for bone tissue engineering applications. *Ceram. Int.* 49(2): 1572–1584. <https://doi.org/10.1016/j.ceramint.2022.10.341>
14. Cahyaningrum S.E., Herdyastuty N., Devina B., Supangat D. 2017. Synthesis and characterization of hydroxyapatite powder by wet precipitation method. *IOP Conf. Series: Mater. Sci. Eng.* 299: 012039. <https://doi.org/10.1088/1757-899X/299/1/012039>
15. Chong R, Fan Y, Du Y, Liu L, Chang Z, Li D. 2018. Hydroxyapatite decorated TiO₂ as efficient photocatalyst for selective reduction of CO₂ with H₂O into CH₄. *Int. J. Hydrogen Energy.* 43(49): 22329–22339. <https://doi.org/10.1016/j.ijhydene.2018.10.045>
16. Dermawan, S.K., Ismail Z.M.H., Jaffri M.Z., Abdullah H.Z. 2022. Effect of the calcination temperature on the properties of hydroxyapatite from black tilapia fish bone. *Journal of Physics.* 1:012034. <https://doi.org/10.1088/1742-6596/2169/1/012034>
17. Dihom H.R., Al-Shaibani M.M., Mohamed R.M.S.R., Al-Gheethi A.A., Sharma A., Khamidun M.H.B. 2022. Photocatalytic degradation of disperse azo dyes in textile wastewater using green zinc oxide nanoparticles synthesized in plant extract: A Critical review. *J. Water Process. Eng.* 47: 102705. <https://doi.org/10.1016/j.jwpe.2022.102705>
18. Fatimah I., Hidayat H., Citradewi P.W., Tamyiz M., Doong R., Sagadevan S. 2023. Hydrothermally synthesized titanium/hydroxyapatite as photoactive and antibacterial biomaterial. *Heliyon.* 9(3): e14434. <https://doi.org/10.1016/j.heliyon.2023.e14434>
19. Ghaly A.E., Ananthashankar R., Alhattab M., Ramakrishna V.V. 2014. Production, characterization and treatment of textile effluents: A Critical review. *J. Chem. Eng. Process. Technol.* 5(1): 1–18. <http://dx.doi.org/10.4172/2157-7048.1000182>
20. Hayashi T., Nakamura K., Suzuki T., Saito N., Murakami Y. 2020. OH radical formation by the photocatalytic reduction reactions of H₂O₂ on the surface of plasmonic excited Au-TiO₂ photocatalysts. *Chem. Phys. Lett.* 739: 136958. <https://doi.org/10.1016/j.cplett.2019.136958>
21. Hossain M.S., Tuntun S.M., Bahadur N.M., Ahmed S. 2022. Enhancement of photocatalytic efficacy by exploiting copper doping in nano-hydroxyapatite for degradation of Congo red dye. *R. Soc. Chem.* 12: 34080–34094. <https://doi.org/10.1039/d2ra06294a>
22. Izzetti R., Genna S., Nisi M., Gulia F., Miceli M., Giuca M.R. 2022. Clinical applications of nano-hydroxyapatite in dentistry. *Appl. Sci.* 12: 10762. <https://doi.org/10.3390/app122110762>

23. Jamil Y.M.S., Awad M.A.H., Al-Maydama H.M.A., Alhakimi A.N., Shakdofa M.M.E., Mohammed S.O. 2022. Gold nanoparticles loaded on TiO₂ nanoparticles doped with N₂ as an efficient electrocatalyst for glucose oxidation: preparation, characterization, and electrocatalytic properties. *J. Anal. Sci. Technol.* 13(54): 1–16. <https://doi.org/10.1186/s40543-022-00363-0>
24. Kumar K.C.V., Subha T.J., Ahila K.G., Ravindran B., Chang S.W., Mahmoud A.H., Mohammed O.B., Rathi M.A. 2021. Spectral characterization of hydroxyapatite extracted from black Sumatra and fighting cock bone samples: A comparative analysis. *Saudi J. Biol. Sci.* 28: 840–846.
25. Kumar C.S., Dhanaraj K., Vimalathithan R.M., Ilaiyaraja P., Suresh G. 2020. Hydroxyapatite for bone related applications derived from sea shell waste by simple precipitation method. *J. Asian Ceram. Soc.* 8(2): 416–429. <https://doi.org/10.1080/21870764.2020.1749373>
26. Latha A., Partheeban P., Ganesan R. 2017. Treatment of textile wastewater by electrochemical method. *Int. J. Earth Sci. Eng.* 10(1): 146–149. <https://doi.org/10.21276/ijee.2017.10.0124>
27. Mancuso A., Lervolino G. 2022. Synthesis and application of innovative and environmentally friendly photocatalysts: A Review. *Catalyst.* 12(10): 1074. <https://doi.org/10.3390/catal12101074>
28. Mirkovic M., Filipovic S., Kalijadis A., Maskovic P., Maskovic J., Vlahovic B., Pavlovic V. 2022. Hydroxyapatite/TiO₂ Nanomaterial with defined microstructural and good antimicrobial properties. *Antibiotics.* 11(592): 1–14. <https://doi.org/10.3390/antibiotics11050592>
29. Musthofa A.M.H., Syafila M., Helmy Q. 2023. Effect of activated carbon particle size on methylene blue adsorption process in textile wastewater. *Indones. J. Chem.* 23(2): 461–474. <https://doi.org/10.22146/ijc.79784>
30. Naik A.S., Mora L., Hayes M. 2020. Characterisation of seasonal mytilus edulis by-products and generation of bioactive hydrolysates. *Appl. Sci.* 10: 6892. <https://doi.org/10.3390/app10196892>
31. Nguyen T.T.V., Anh N.P., Ho T.G.T., Pham T.T.P., Nguyen P.H.D., Do B.L., Huynh H.K.P., Nguyen T. 2022. Hydroxyapatite derived from salmon bone as green ecoefficient support for ceria-doped nickel catalyst for CO₂ methanation. *ACS Omega.* 7: 36623–36633. <https://doi.org/10.1021/acsomega.2c04621>
32. Noviyanti A.R., Asyiah E.N., Permana M.D., Dwiyanti D., Suryana., Eddy D.R. 2022. Preparation of hydroxyapatite-titanium dioxide composite from eggshell by hydrothermal method: Characterization and antibacterial activity. *Crystals.* 12(11):1–15. <https://doi.org/10.3390/cryst12111599>
33. Odabaşı U.S., Boudraà I., Aydin R. 2022. Photocatalytic removal of pharmaceuticals by immobilization of TiO₂ on activated carbon by LC–MS/MS monitoring. *Water Air Soil Pollut.* 233:111. <https://doi.org/10.1007/s11270-022-05579-9>
34. Ojha P., Shrivastava R. 2023. Electrochemical oxidation of textile effluents and further treatment by coupled system electrooxidation using prosopis cineraria. *Indian J. Chem. Technol.* 30:242-246. <https://doi.org/10.56042/ijct.v30i2.69010>
35. Oyetade J.A., Machunda R.L., Hilonga A. 2022. Photocatalytic degradation of azo dyes in textile wastewater by Polyaniline composite catalyst: A Review. *Sci. Afr.* 17:1–27. <https://doi.org/10.1016/j.sciaf.2022.e01305>
36. Pai S., Kini M.S., Mythili R., Selvaraj R. 2022. Adsorptive removal of AB113 dye using green synthesized hydroxyapatite/magnetite nanocomposite. *Environ. Res.* 210: 112951. <https://doi.org/10.1016/j.envres.2022.112951>
37. Qutub N., Singh P., Sabir S., Sagadevan S., Oh W.C. 2022. Enhanced photocatalytic degradation of acid blue dye using CdS/TiO₂ nanocomposite. *Sci. Rep.* 12: 5759. <https://doi.org/10.1038/s41598-022-09479-0>
38. Raj S., Singh H., Bhattacharya J. 2023. Treatment of textile industry wastewater based on coagulation-flocculation aided sedimentation followed by adsorption: Process studies in an industrial ecology concept. *Sci. Total Environ.* 857(2): 159464. <https://doi.org/10.1016/j.scitotenv.2022.159464>
39. Rajabi H.R., Sajadiasl F., Karimi H. 2020. Green synthesis of zinc sulfide nano photocatalysts using aqueous extract of Ficus Johannis plant for efficient photodegradation of some pollutants. *J Mark Res.* 9: 15638–15647. <https://doi.org/10.1016/j.jmrt.2020.11.017>
40. Reddy A.S., Kalla S., Murthy Z.V.P. 2022. Textile wastewater treatment via membrane distillation. *Environ. Eng. Res.* 27(5): 1–16. <https://doi.org/10.4491/eer.2021.228>
41. Ren G., Han H., Wang Y., Liu S., Zhao J., Meng X., Li Z. 2021. Recent Advances of Photocatalytic Application in Water Treatment: A Review. *Nanomaterials.* 11(7): 1804. <https://doi.org/10.3390/nano11071804>
42. Sahoo C., Panda B.B., Gupta A.K. 2022. Design aspects of a continuous flow photocatalytic reactor and its application to degrade methylene blue and textile wastewater. *Chem. Eur.* 7(38): e202201179. <https://doi.org/10.1002/slct.202201179>
43. Sastrawidana D.K., Rachmawati D.O., Sudiana K. 2018. Color removal of textile wastewater using indirect electrochemical oxidation with multi carbon electrodes. *EnvironmentAsia* 11(3), 170-181. <https://doi.org/10.14456/ea.2018.46>

44. Siddiqui S.I., Allehyani E.S., Al-Harbi S.A., Hasan Z., Abomuti M.A., Rajor H.K., Oh S. 2023. Investigation of Congo Red Toxicity towards Different Living Organisms: A Review. *Processes*. 11(3): 807. <https://doi.org/10.3390/pr11030807>
45. Sirajudheen P., Kasim V.R., Nabeena C.P. 2021. Tunable photocatalytic oxidation response of ZnS tethered chitosan-polyaniline composite for the removal of organic pollutants: A mechanistic perspective. *Mater Today* 47: 2553–2559. <https://doi.org/10.1016/j.matpr.2021.05.054>
46. Solonenko A.P., Shevchenko A.E., Rozdestvensky A.A., Dzyuba G.G. 2022. Investigation of the process and products of calcination of composite granules based on hydroxyapatite, wollastonite and gelatine. *IOP Conf. Ser.: J. Phys.* 2182: 012081. <https://doi.org/10.1088/1742-6596/2182/1/012081>
47. Sudiana I.K., Citrawathi D.M., Sastrawidana I.D.K., Sukarta I.N., Wirawan G.A.H. 2022. Biodegradation of turquoise blue textile dye by wood degrading fungi isolated from a plantation area. *J. Ecol. Eng.* 23(7), 205–214. <https://doi.org/10.12911/22998993/150044>
48. Sukarta I.N., Ayuni N.P.S., Sastrawidana I.D.K. 2021. Utilization of khamir (*Saccharomyces cerevisiae*) as adsorbent of remazol red RB textile dyes. *Ecol. Eng. Environ. Technol.* 22(1):117–123. <https://doi.org/10.12912/27197050/132087>
49. Syafira R.S., Devi M.J., Gaffar S., Hartati Y.W. 2023. Immobilization of biomolecules on hydroxyapatite and Its composites in biosensor application: A Review. *Biointerface Res. Appl. Chem.* 13(5): 1–17. <https://doi.org/10.33263/BRIAC135.499>
50. Touati A, Hamed T, Najjar W, Ksibi Z, Sayadi S. 2016. Photocatalytic degradation of textile wastewater in presence of hydrogen peroxide: Effect of cerium doping titania. *J. Ind. Eng. Chem.* 35(25):36–44. <https://doi.org/10.1016/j.jiec.2015.12.008>
51. Ummartyotin S., Tangnorawich B. 2015. Utilization of eggshell waste as raw material for synthesis of hydroxyapatite. *Colloid Polym. Sci.* 239: 2477–2483. <https://doi.org/10.1007/s00396-015-3646-0>
52. Vital-Grappin A.D., Ariza-Tarazona M.A., Luna-Hernández V.M., Villarreal-Chiu J.F., Hernandez-Lopez J.M., Siligardi C., Cedillo-González E.I. 2021. The Role of the reactive species involved in the photocatalytic degradation of HDPE microplastics using C, N-TiO₂ powders. *Polymers*. 13(7):1–18. <https://doi.org/10.3390/polym13070999>
53. Wardhani S., Rahman M.F., Purwonugroho D., Tjahjanto R.T., Damayanti C.A., Wulandari I.O. 2016. Photocatalytic degradation of methylene blue using TiO₂- natural zeolite as a photocatalyst. *J. Pure appl. Chem. Res.* 5(1): 19–27. <http://dx.doi.org/10.21776/ub.jpacr.2016.005.01.232>
54. Wu S.C., Hsu H.C., Wang H.F., Liou S.P., Ho W.F. 2023. Synthesis and characterization of nano-hydroxyapatite obtained from eggshell via the hydrothermal process and the precipitation method. *Molecules*. 28(492): 1–13.